Study of the effect of polyacrylic acid dispersant on magnetite deposits in steam generators conditions

Ricardo d'Angelo, Marion Roy, Thierry Pauporte, Sophie Delaunay, Dominique You, Carine Mansour, Frédéric Miserque, Francois Foct

Study of the Effect of Polyacrylic Acid Dispersant on Magnetite Deposits in Steam Generators Conditions.

Ricardo D'ANGELO[a,b,1], Marion ROY[c]*, Thierry PAUPORTÉ[b]*, Sophie DELAUNAY[a], Dominique YOU[c], Carine MANSOUR[a], Frédéric MISERQUE[d], François FOCT[a]

[a] *EDF Lab, Chemistry and Materials for Energy Efficiency Group, Avenue des Renardières, 77818 Moret-sur-Loing Cedex, France*

[b] *PSL Research University, Chimie ParisTech – CNRS, Institut de Recherche de Chimie Paris, UMR8287, 11 rue Pierre et Marie Curie, 75005 Paris, France.*

[c] *Den-Service d'Etude du Comportement des Radionucléides (SECR), CEA, Université Paris-Saclay, F-91191, Gif-sur-Yvette, France.*

[d] *Den-Service d'Etude de Corrosion et du Comportement des Matériaux dans leur Environnement (SCCME), CEA, Université Paris-Saclay, F-91191, Gif-sur-Yvette, France*

*Corresponding authors: marion.roy@cea.fr; thierry.pauporte@chimie-paristech.fr

ABSTRACT

The present paper aims at determining and understanding the curative effect and action mode of polyacrylic acid (PAA) dispersant on magnetite (Fe_3O_4) deposits on Inconel tubes in the conditions found in steam generators (SGs). Magnetite deposits produced by electrodeposition on Inconel 600TT and 690TT have been used as model layers and exposed to various concentrations of PAA in a high pressure and temperature dedicated experimental loop. Measurements of iron concentration and post-test deposit characterizations have been performed. They show the solubilization of iron by the dispersant and clarify its effect on the chemical, morphological and structural properties of the layers.

Keywords

Polymer; Electrodeposited films; Oxide coatings; XPS; TEM

[1] *Present address : Systèmes Stekar inc. 668, 5e Avenue, Beauceville (Québec) G5X 1L6 Canada, ricardo.dangelo@stekar.com*

1. Introduction

The deposition of corrosion products (CPs) in steam generators (SG) promotes the fouling of SG tubes and the blockage of the broached tube support plates of SG units. These CPs, composed primarily of magnetite, are generated by the corrosion of the secondary circuit components of nuclear Pressurized Water Reactors (PWRs) and are transferred by the water flow. The fouling and the blockage of SGs decrease their thermal efficiency and increase the maintenance costs.

In order to limit these phenomena, two strategies are developed dealing with the current chemical conditioning of the secondary side and studies are in progress for: (i) the use of chemical cleaning techniques [1], [2] and (ii) the injection of a chemical additive as dispersant [3–5].

The effects of dispersant injection at the nuclear power plant scale has been already investigated by both short term trials (STT) and long term trials (LTT) [6–8]. The tested dispersant was a polyacrylic acid (PAA) of high molecular weight, dissolved in a solution neutralized with ethanolamine (OptiSperse PWR6600, General Electric). The results obtained for STT and LTT indicated an increase in the average SG blowdown iron removal efficiency ranging from 1-2 % to 20-60 % for STT and from 5 % to 45-50 % for LTT [6–8]. After these promising results, a first trial of dispersant injection was conducted by Electricité de France (EDF) company at the Golfech 2 nuclear power plant from 2012 to 2014 using a PAA solution neutralized with morpholine (OptiSperse PWR6610, General Electric). However, prior to implement the online addition of this dispersant to all power plant units, further studies must be performed to better evaluate and understand the curative effect of PAA on the blockage and the fouling of the SGs. PAA was chosen because of the good feedback, gathered worldwide, after its injection in SG . Moreover, it seems that this dispersant is efficient but does not have a negative impact on the physical-chemical parameters followed (pH and cationic conductivity) in the secondary circuit of nuclear power plants.

The observation and characterization of the oxide layers formed by static means on the SG tube materials in the presence and in the absence of PAA are necessary to determine the complexing and/or dispersing effects of PAA on the fouling deposits present on oxidized SG tubes. The objectives of this work were to determine if PAA dissolves magnetite deposits under physico-chemical conditions close to those encountered in SGs and to clarify the action

mode and the efficiency of PAA on the fouling and blockage deposits in SGs. The potential curative effects of PAA on magnetite deposits formed on the nickel base alloys, Inconel 600TT and 690TT have been investigated. These materials have been chosen because historically the Inconel 600TT was one of the grade used to elaborate the SG tubes but nowadays it was replaced in a large extent by the Inconel 690TT. The study was more detailed for the last grade since it is the most used alloys for SG tubes in PWR.

The effectiveness of PAA was evaluated by the determination of the following parameters by diverse techniques of analysis: (i) the evolution of iron concentration in solution, (ii) the interaction of PAA with the oxide and, (iii) the modification of the morphology of the oxide layer. Moreover, the study has been performed on pre-existing model magnetite deposits formed by cathodic electrodeposition from an alkaline Fe(III)-triethanolamine (TEA) electrolytic solution on Inconel substrates [9]. In this study, the electrodeposited magnetite layers (EDMLs) are models for the investigation of the effect of PAA on the magnetite layers formed in the SG of nuclear pressurized water reactors. Indeed, our published works [1], [9] have shown that the deposits formed in SG conditions are close to the electrodeposited ones. EDMLs have been used since they have the advantage of being easier and faster to produce compared to the former layers.

Experimental conditions are first described with the samples used and the operation of the experimental loop. Four tests were performed with identical flow and physico-chemical conditions, but with different PAA concentrations. The results obtained from these tests carried out in the loop are then detailed and discussed. To determine the effectiveness of PAA on the magnetite deposits, iron release in the solution was quantified by samplings performed at the loop inlet and exit. Moreover, the effects of PAA at various concentrations on oxide layers were characterized and compared.

The novelty of this work is mostly in the methodology. First, the interaction between PAA and magnetite in thermal-chemical conditions of the secondary circuit of PWR, in a broad range of PAA concentration was not studied yet. Secondly, the impact of PAA on the chemistry of the secondary conditioning combined to the study of its impact on the morphology and structure of the oxide layer are complementary. Moreover, the presence of PAA on the oxide surface after the tests is studied. The combination of those results gave some leads on the interaction mechanism of PAA with magnetite layers close to those in SG.

2. Experimental

2.1. Substrate materials

The substrate materials used were Inconel alloys of both 600TT and 690TT grades, in the forms of tube segments and plates. The plates were of dimensions 20×10×2 mm and the tube segments had a height of 20 mm and external diameters of 22.20 mm and 19.05 mm for 600TT and 690TT, respectively. The tubes and plates had exactly the same chemical composition for each Inconel grade. They are summarized in Table 1.

Alloy	Ni	Cr	Fe	C	Mn	P	S	Si	Cu	Co	Al	Ti
600TT *RCC-M 4101*	> 72.0	14.0 – 17.0	6.0 – 10.0	0.01 – 0.05	1.0	0.025	0.015	0.5	0.5	0.1	0.5	0.5
690TT *RCC-M 4105*	> 58.0	28.0 – 31.0	7.0 – 11.0	0.01 – 0.04	0.5	0.025	0.015	0.5	0.5	0.1	0.5	0.5

Table 1: Chemical compositions (in weight %) of Inconel 600TT and 690TT alloys.
The associated specifications are in italic [8].

2.2. Magnetite film preparation

Electrodeposition has been shown a powerful technique to prepare iron oxides in a controlled manner, especially magnetite (Fe_3O_4) [9–17]. Magnetite layers were deposited on both plates and tube segments by cathodic electrodeposition following the process developed by Goujon *et al.* [9]. The substrates were first mechanically polished using SiC papers with P320, P600 and P1200 decreasing grain sizes, carefully cleaned with soap and rinsed with deionized water prior to be sonicated 5 min in acetone and 5 min in ethanol. The electrochemical depositions were carried out in a three-electrode glass cell at an applied potential of -1.05 V versus the saturated calomel electrode (SCE) for 2000 s [18] to achieve a thickness of about 12-14 μm [9]. The reference electrode was a SCE (with potential at +0.25 V versus the normal hydrogen electrode (NHE)) placed in a separate compartment maintained at room temperature. The counter-electrode (CE) was a platinum wire for the plate samples and a platinum cylinder for the Inconel tube segments [19]. To ensure a deposition as homogeneous as possible, the plates were fixed in front of, and the tube segments in the center of the CE. A magnetic barrel was used at a rotating speed of 170 rpm to homogenize the solution. The deposition medium was prepared with MilliQ quality water (18.2 MΩ

cm). 1.3 g of Fe(III) sulfate hydrate was dissolved in 7.5 ml of 1 M TEA. This solution was diluted with 25 ml of water. It was then added to a second solution of 6.0 g of sodium hydroxide (NaOH) in 42.5 ml of water at 80 °C. The resulting solution pH was 12.5 at 25 °C. After deposition, the deposit was rinsed with deionized water and then dried in air. XRD characterizations confirmed the deposition of a pure magnetite film on nickel base alloys, as described in the literature [9].

2.3. PAA effect study

Four different PAA concentrations (0, 0.1, 1 and 10 $mg.kg^{-1}$) were investigated on EDMLs deposited on the two kinds of Inconel alloys. The duration of each test was one month (Table 2). The molecular weight of the PAA product used (M_{PAA}) was determined to range between 123 000 Da and 132 000 Da [20].

21

[PAA] Theoretical ($mg.kg^{-1}$)	**[PAA] Tested** ($mg.kg^{-1}$)	**Duration** (h)	$\mathbf{T_{reactor}}$ (°C)	$\mathbf{P_{reactor}}$ (Pa)	$\mathbf{Q_L}$ ($g.h^{-1}$)	$\mathbf{t_{residence}}$ (min)
0	0	745	275	8×10^6	54.6 ± 0.1	[20-56]
0.1	0.10 ± 0.02	745	275	8×10^6	54.8 ± 0.1	[20-56]
1	1.01 ± 0.01	737	275	8×10^6	55.4 ± 0.5	[20-56]
10	10.02 ± 0.01	746	275	8×10^6	54.7 ± 0.3	[20-56]

Table 2: Matrix describing the PAA concentrations, duration and physico-chemical conditions for tests.

To evaluate the effect of PAA on the pre-existing magnetite deposits, studies were performed in physico-chemical conditions representative of the SGs. Experiments were performed by inserting the magnetite deposited samples within the GROZIE once-through type loop [21]. This loop was designed to reproduce the operating conditions in the secondary circuit (except the thermohydraulic conditions), while maintaining only liquid phase. A schematic of the GROZIE experimental loop is shown in Figure 1. The entirety of this system did not contain iron and was made of titanium alloy in order to be inert with respect to the studied chemical medium.

The samples were exposed to deaerated water (pH 9.6 at 25 °C; adjusted by addition of ammonia NH_4OH, 25 vol%) containing chemical conditioning used in the SG: morpholine (5.5 $mg.kg^{-1}$) and ammonia (between 1.5 $mg.kg^{-1}$ and

2.6 mg.kg^{-1}). To obtain an oxygen free medium and a reducing redox conditions, the solutions were maintained under pressure (0.2 MPa) of a mixture of argon and dihydrogen gas (Ar-5 vol% H_2). The pressure of the loop was 8 MPa and its temperature was 275 °C. At the outlet, the solution was measured to follow the iron concentration, pH and the total conductivity of the solution. The chemistry was controlled by solution sampling done at the entrance and exit of the loop. The solution samples taken at the loop exit were analyzed after a filtration through a 0.45 µm pore sized filter.

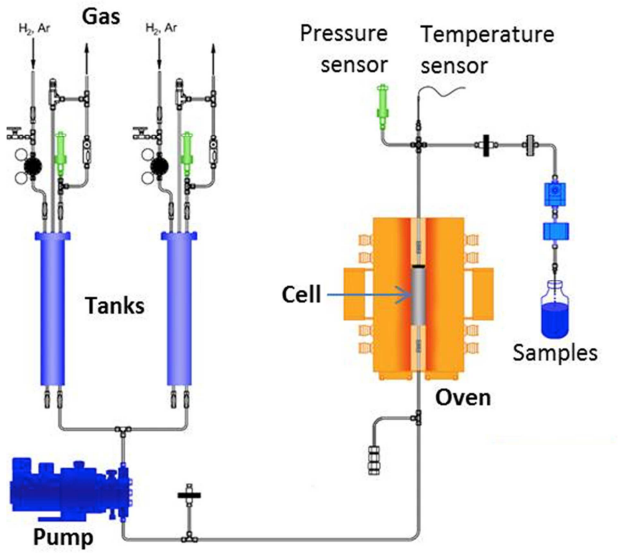

Figure 1: Schematic of the experimental GROZIE loop dedicated to the study of the curative effect of PAA [21]

The autoclave dimensions were 180 ml in volume and 360 mm in length. The samples were fixed to an inert sample holder made of titanium alloy (TA6V) as shown in Figure 2. It allowed a combination of plates and tube segments to be placed for each test in the autoclave. The flow rate, and thus the residence time of the solution within the autoclave, is a function of the autoclave cell volume and of the volumetric mass of water at 275 °C and 8 MPa. The solution residence time was fixed to be 20 min at the autoclave entrance, but evolved along the length of the autoclave with the first plates having a 25 min residence time and the top tube 55 min. This parameter is given by the following equation:

$$t_{residence,n} = t_{residence,n-1} + \frac{\rho_w V_{free,n}}{Q_L} \qquad \text{with } t_{residence,0} = 0 \qquad (1)$$

where $t_{residence,n}$ is the residence time at section *n* (min), $t_{residence,n-1}$ is the residence time in the section *n-1* (min), ρ_w is

the density of water (kg.m^{-3}), $V_{free,n}$ is the free volume *i.e.* the volume of water at the section n (m^3) and Q_L is the liquid mass flow (kg.min^{-1}).

This was done to ensure that samples were exposed at least 20 min to PAA which is in the same order of magnitude with the residence time of solution in SGs and allows to enhance the interaction with PAA. After completing each test, the samples were placed in a desiccator to avoid the pollution of the layers by nitrogen and carbon prior to analysis.

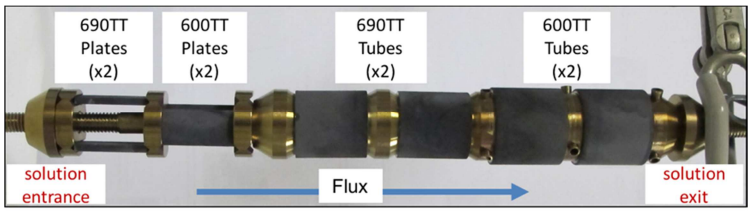

Figure 2: GROZIE loop sample holder with samples mounted. The sample holder is placed vertically inside the autoclave and the solution enters in the autoclave from the bottom.

Iron concentration measurements were performed using atomic absorption spectroscopy (AAS). The spectrometer used for these analyses was a VARIAN SpectrAA-800 equipped with graphite tube atomizers. Solution samples were collected for analysis in flasks containing a drop of ultra-pure nitric acid in order to avoid precipitation of iron when exposed to air and/or absorption on the walls. AAS measurements were performed on solution samples collected at the entrance and at the exit of the GROZIE loop to evaluate the total iron quantity and then to assess whether PAA at various concentrations has a curative effect on pre-existing magnetite deposits. Between 8 and 17 samples were collected periodically during each of the four experiments.

2.4 Oxide layer characterizations

Sample morphologies were examined with a high resolution Sigma Zeiss scanning electron microscope in the secondary electron mode (SEM-SE) at an acceleration voltage of 5 kV. X-ray diffraction (XRD) analysis of each sample, before and after experiments, was performed using a X'Pert PANalytical diffractometer with Cu-Kα radiation (λ =1.5406 Å). Extreme surface chemical analyses were measured by X-ray photoelectron spectroscopy (XPS) using Thermofisher Escalab 250 xi spectrometer equipped with a monochromatized Al Kα ($h\nu$ = 1486.6 eV)

X-ray source. High Angle Annular Dark-Field Scanning Transmission Electron Microscopy (HAADF-STEM) observations and electronic micro-diffraction analyses were performed using a Tecnai Osiris microscope at an acceleration voltage of 200 kV.

3. Results and discussion

3.1 Effect of PAA on iron concentration in solution

The results of AAS measurements performed at the entrance and at the exit of the loop to quantify the total iron concentrations are gathered in Table 3.

	0 mg.kg^{-1} PAA		**0.1 mg.kg^{-1} PAA**		**1 mg.kg^{-1} PAA**		**10 mg.kg^{-1} PAA**	
	[Fe] In	[Fe] Out	[Fe] In	[Fe] Out	[Fe] In	[Fe] Out	[Fe] In	[Fe] Out
[min, max]	< 0.54 **	< 0.54	[<0.54, 1.8]	[< 0.54, 3.9]	[< 0.54, 1.5]	[< 0.54, 13.9]	[< 0.54, 2.0]	[4.1, 143.2]
Average ($\times10^{-6}$ g.kg^{-1})*	< 0.54	< 0.54	1.1	1.5	< 0.54	7.0	< 0.54	83.6
Standard Deviation	-	-	1.3	1.3	< 0.54	4.4	< 0.54	24.4

*Each value indicated is the average of 8 to 17 samples, dependent on the test.
** The limit of detection of iron is 0.54×10^{-6} g.kg^{-1} in AAS

Table 3: Measurements of iron concentration values at the entrance and exit of the GROZIE loop, for the four tests at various PAA concentrations.

They showed that without PAA addition, iron concentrations were measured below the limit of detection of the instrument (*i.e.* 0.54×10^{-6} g.kg^{-1}). The test with 0.1 mg.kg^{-1} PAA showed no clear increase in iron concentration at the exit, considering the uncertainty of the measurement ($\pm 0.5\times10^{-6}$ g.kg^{-1}). However, tests using 1 mg.kg^{-1} and 10 mg.kg^{-1} of PAA demonstrated a clear increase in the iron concentration at 7×10^{-6} g.kg^{-1} and 83×10^{-6} g.kg^{-1}, respectively. These values were then used to plot the evolution of the concentration of iron measured after interacting with PAA as a function of the PAA concentration introduced for the performed tests (Figure 3). A linear augmentation is observed from the three tests with different concentrations of PAA between 0.1 and 10 mg.kg^{-1}. However in order to confirm this linear dependence over a broad range PAA concentration, a fifth test was performed with 500 mg.kg^{-1} of PAA in the same thermal-chemical conditions. For this last test, the average iron concentration measured was 4650×10^{-6} g.kg^{-1}. This result was added to the other tests results in Figure 3. Then a

linear dependence is clearly observed over 4 order of magnitude of PAA concentration. The expression is indicated below:

$$[\mathrm{Fe}](10^{-6}\,\mathrm{g.\,kg^{-1}}) = 0.95 log_{10}[\mathrm{PAA}](10^{-6}\,\mathrm{g.\,kg^{-1}}) - 1.8$$

From these analyses, we are able to conclude that there was no clear effect of PAA on the oxide layer after the test at 0.1 mg.kg^{-1} PAA whereas a clear curative effect of PAA after the tests at 1, 10 and 500 mg.kg^{-1} PAA is found. The iron concentration, measured at the exit of GROZIE, increased linearly with increasing the PAA concentration.

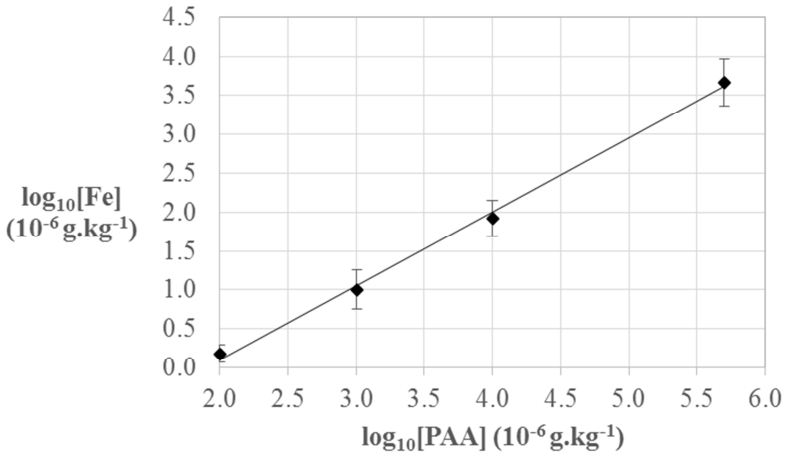

Figure 3: Evolution of the average concentration of iron measured at the exit of GROZIE after interaction with PAA, for the performed tests with a concentration of PAA ranging between 0.1 and 500 mg.kg^{-1}. The points are the mean values and the lines are the error bars corresponding to the standard deviation.

3.2 Effect of PAA on oxide deposits

Iron concentration measurements have shown that PAA has a significant curative effect at concentrations above 1 mg.kg^{-1}. It is assigned to the complexation of iron ions by the carboxylate groups of the PAA polymer [22–26]. It remains to be determined the action mechanisms by which the PAA interacts with the magnetite deposits.

The surface of the oxide layers was observed by SEM after each test at different concentrations of PAA to determine the morphological changes in the oxide surface (Figure 4). These observations were also compared to those of a reference sample, not placed in the loop (Figure 4, a). The comparison of the surface oxide for the four tested

samples with the reference sample shows that the oxide present on the reference sample, made of crystallites with smooth {111} planes and well-defined octahedral shape, changed in appearance. For the test without PAA, roughness of the {111} planes has increased. Closer examination of the individual octahedra for this test (Figure 4, b) shows the removal of layers of the {111} octahedral facets. These results indicate an effect of the circuit (temperature, conditioning and flow rate) on the plates and provide evidence that the magnetite octahedra dissolved in the solution.

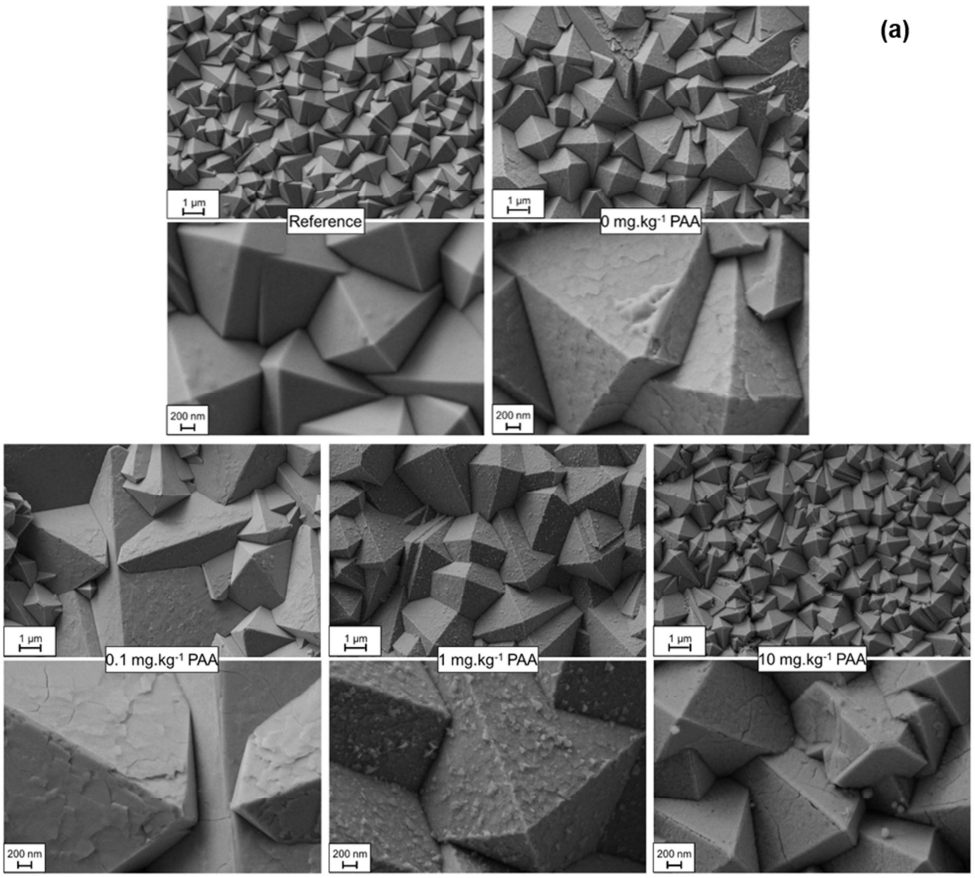

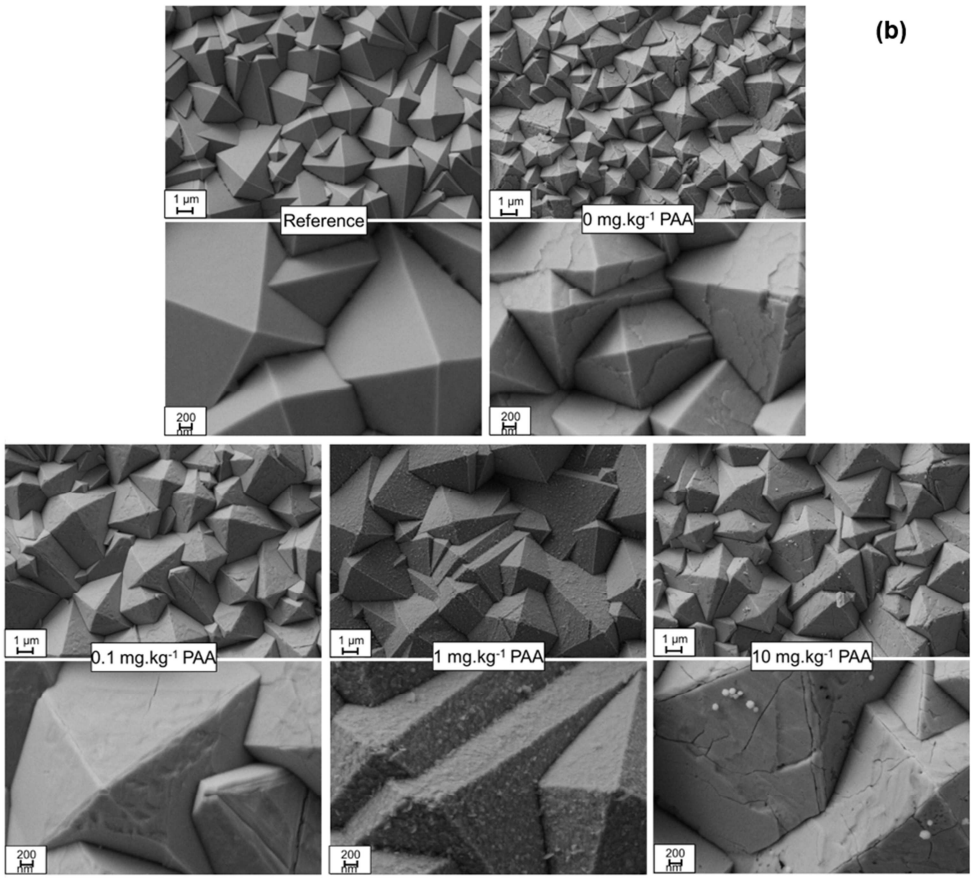

Figure 4: SEM-SE pictures of the surface of magnetite layers deposited on Inconel 690TT (a) and Inconel 600TT (b) plates for reference, test without PAA, 0.1 mg.kg^{-1} PAA, 1 mg.kg^{-1} PAA and 10 mg.kg^{-1} PAA.

The addition of PAA was found to produce similar increases in roughness as the test without PAA but in a much higher degree. There is also a localized diminution of the octahedral peak corners, which is not apparent at the octahedron bases. This can be observed for both the low (0.1 mg.kg^{-1}) and high (10 mg.kg^{-1}) PAA concentration tests. This may be a result of the accessibility of the polymer and thus of the interaction of the PAA molecules with the oxide surface. It is possible that a gradient in the PAA concentration occurs with the peaks being constantly renewed by the conditioned solution while the base of the octahedra have a reduced renewal of solution. As a consequence, the peaks are reduced faster than the bases. The molecular weight of the polymer would also need to be taken into account, as the specific chain length would require that it be bent or partially degrade in order to approach and interact with the base of the octahedral crystallites. Closer examination of the octahedra after tests at 0.1 and 10

mg.kg^{-1} (Figure 4, (a) and (b)) proves this interpretation. From these observations, it seems that there is a preferential adsorption, in particular at the octahedral peak corners. Joshi *et al.* [27] observed the possibility of preferential adsorption on certain oxide planes in their study on the effect of PAA addition on the oxides formed on carbon steel surfaces. The carbon steel samples were oxidized at high temperature (200 - 250 ºC) and high pressure (1.4 - 4 MPa) for 20 days in a titanium lined stainless steel autoclave containing deaerated water conditioned with SG additives in the presence and absence of PAA. Observations made on samples in the presence of varying concentrations of PAA (0 - 700×10^{-6} g.kg^{-1}; 10^{6} g.mol^{-1} molecular weight) indicated a magnetite oxide layer with changes in the magnetite octahedral crystallization, which led Joshi *et al.* [27] to hypothesize that the PAA molecule adsorbs to preferred planes of the oxide lattice and hinders the growth of certain planes of oxide.

In this study, in addition to having a localized diminution of the octahedral peaks, both tests at 1 mg.kg^{-1} and 10 mg.kg^{-1} led to the formation of surface layers onto the magnetite octahedra after testing with PAA. For the case of 10 mg.kg^{-1} this was most notable on Inconel 690TT plates (Figure 5), possibly because of their position in the autoclave, since they were the first samples that interacted with PAA of the largest molecular size. The surface layer was present predominantly on the octahedral peaks and was sparse between neighboring octahedral peaks, in the valleys (Figure 5). Their initial qualitative examinations by EDS indicated the presence of iron, oxygen and titanium. The titanium was determined to be a contamination from the GROZIE autoclave and sample holder, also composed of titanium alloy.

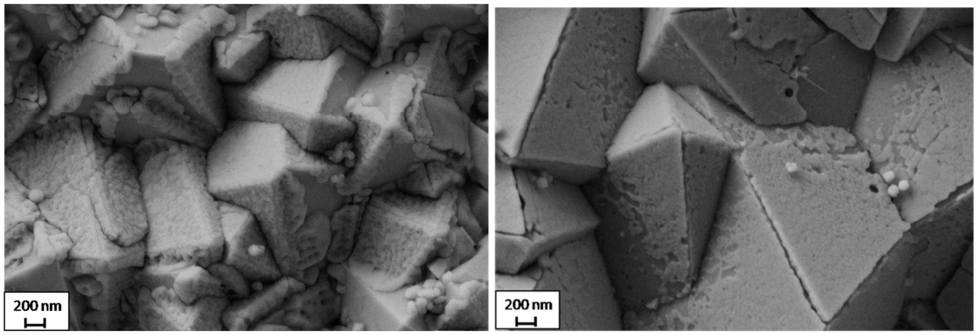

Figure 5: SEM observation of oxide surface after exposure to 10 mg.kg^{-1} PAA for Inconel 690TT plates.

Continuing with the characterization of the layer formed on the magnetite, the samples were analyzed using XRD. Since magnetite samples were prepared using the same reproducible electrochemical method, the XRD patterns were compared to each other after testing. Figure 6 shows the XRD patterns for Inconel 690TT coated substrates after the

four tests and are compared to a reference sample not placed in the loop. These XRD patterns show magnetite peak intensity changes after the tests with and without PAA. However, these changes are difficult to analyze because they occur either in the presence or in the absence of PAA.

Upon completion of the experiment at 10 $mg.kg^{-1}$ PAA, the samples were observed to have formed another oxide phase identified as hematite (α-Fe_2O_3) and indicated by the orange indices in Figure 6. This change, however, was not apparent for tests at 0, 0.1 and 1 $mg.kg^{-1}$. Comparisons were made, between Inconel 690TT and Inconel 600TT, regarding the effect of the sample position on the formation of hematite. It was observed that the first samples interacting with the PAA, Inconel 690TT, had more apparent peaks of hematite present than Inconel 600TT samples. Two hypotheses are considered to explain the formation of hematite:

1. The first hypothesis links the formation of hematite to an interaction of PAA with the iron(II) [28] in the water (Eq. 1). Iron(II) was complexed by PAA shifting the equilibrium towards the right and thus iron(III) in solution precipitated as hematite which could have been deposited on the surface.

$$Fe^{II}Fe_2^{III}O_4 + H_2O + PAA \leftrightarrow PAA \cdot Fe^{2+} + \alpha - Fe_2O_3 + 2OH^- \quad (1)$$

2. The second possibility is that the thermal degradation of PAA produces localized oxidizing conditions, which in turn oxidize the magnetite into hematite. Previous tests in the same physico-chemical conditions were performed to identify and quantify the decomposition products of PAA but with a higher concentration of PAA [29]. It has been found that the main thermal degradation products of PAA are carboxylates: acetate and to a lesser extent formate and propionate. Besides, some carbon dioxide and carbon monoxide are produced. The formation of these last species could create localized oxidizing conditions.

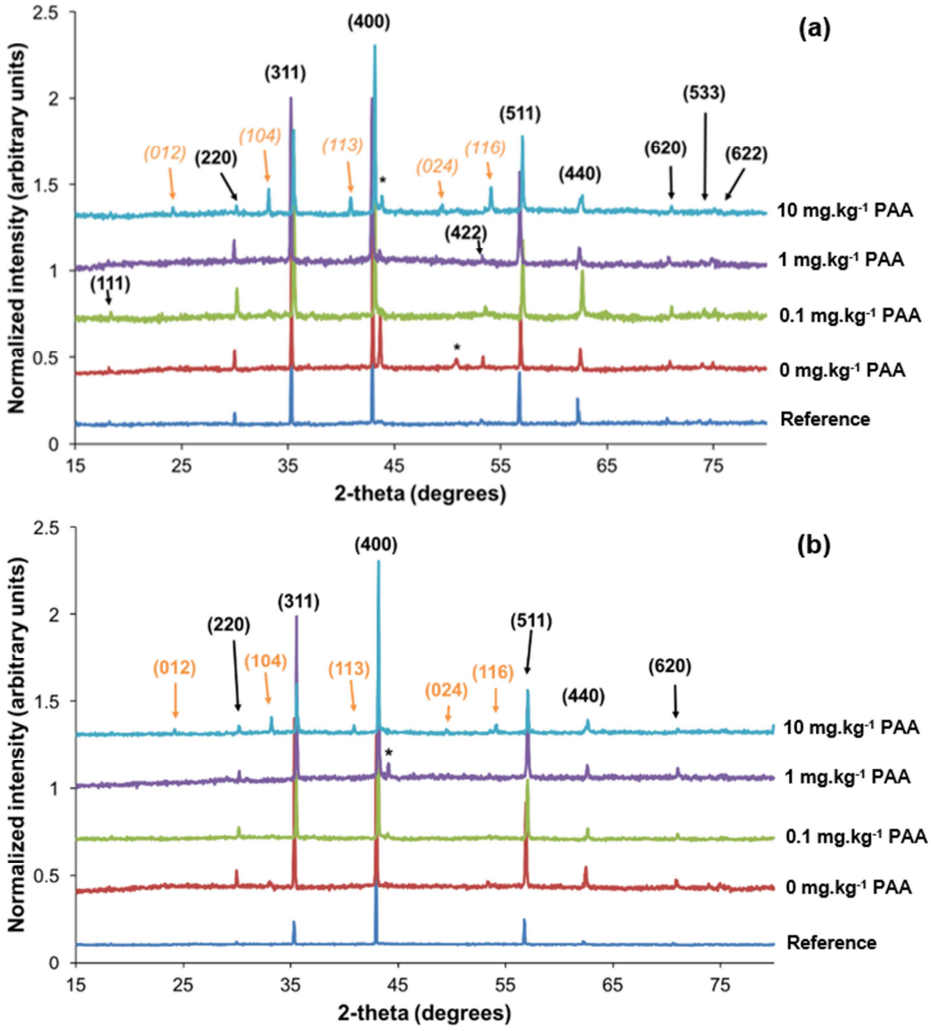

Figure 6: XRD diffraction patterns (λ =1.5406 Å) for coated Inconel 690TT (a) and Inconel 600 (b) plates reference and tests performed in the absence and presence of PAA at different concentrations, the indices in orange italic and black bold indicate hematite and magnetite planes, respectively. The * labels indicate peaks corresponding to the Inconel substrate.

From the SEM observations and XRD analyses it was determined that PAA has an effect on the surface morphology of the magnetite. This was observed by the localized diminution of the octahedral peaks corners. However XRD analyses of samples from the test at 10 $mg.kg^{-1}$ indicated the presence of hematite. XPS surface analyses were conducted to determine whether thin hematite layers, which cannot be detected by XRD, are actually present or not at the lowest concentrations of PAA. Initial XPS analyses were done to determine if a change in the iron oxide

spectra occurred. XPS analyses were performed on samples from tests with 0, 0.1 and 10 mg.kg^{-1} PAA. The analyses were done at the earliest convenience to avoid any modification of the extreme surface of the samples. The narrow scan spectra for Fe 2$p_{3/2}$ peaks for all tests and a reference sample not placed within the loop are shown in Figure 7 for Inconel 690TT. From these curves a change is observed in the shape of the Fe 2$p_{3/2}$ envelope after testing the magnetite sample in the GROZIE loop with and without PAA.

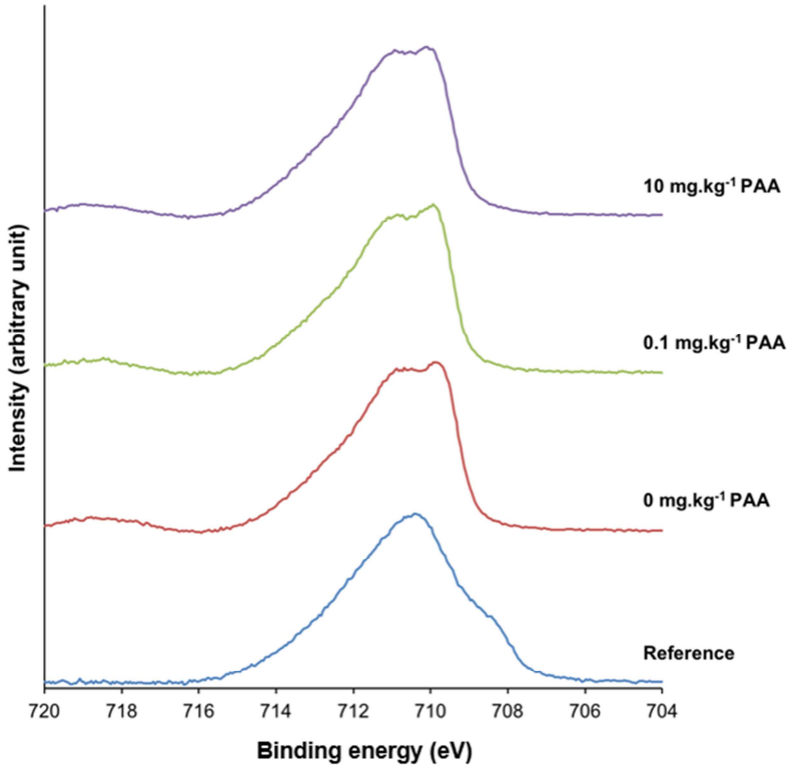

Figure 7 : Narrow scan XPS spectra of Fe 2*p* zoomed into the Fe 2$p_{3/2}$ envelope for the reference sample and samples Inconel 690TT tested in the presence of 0 mg.kg^{-1} PAA, 0.1 mg.kg^{-1} PAA and 10 mg.kg^{-1}.

To understand the difference in the iron structure for all the tests, the narrow scan for the reference sample and the test without PAA were fitted to show the iron(II) and iron(III) multipeaks. Figure 8 shows the Fe 2$p_{3/2}$ peak after (a) and before (b) exposure to secondary chemistry. The background of the spectrum was subtracted using a Shirley background for the Fe 2$p_{3/2}$ envelope. The Fe 2$p_{3/2}$ envelope was fit using peaks corresponding to the 'Gupta and Sen' multiplets [30], [31], surface structures and shake up related satellites. The corresponding multipeak parameters used for the envelope fit can be found in the article by Grosvenor *et al.* [32] who investigated the multiplet splitting

of Fe 2*p* XPS spectra and bonding in iron compounds. Before experimentation, the reference sample was composed of both Fe(III) and Fe(II) multiplets that are characteristic of magnetite deposits [32]. The Fe(III)/Fe(II) ratio was found to be approximately 3:1, which is larger than the expected theoretical ratio of 2:1 and experimental ratio 1.7:1 obtained by Grosvenor *et al.* [32]. Now considering that the XPS analyses are limited to the first 10 nm, with the first 2 to 3 nm being most sensitive, the presence of Fe(III) on the surface of the plates is probably due to the oxidation of the extreme outer layer of the deposit of magnetite and oxygen enrichment after the electrochemical deposition. After the test without PAA, (Figure 8 (a)), the Fe(II) multiplet peaks are no longer present in the Fe $2p_{3/2}$ envelope and there is the appearance of a Fe(III) satellite peak. The loss of the Fe(II) multiplet peaks is assigned to the complete oxidation of the extreme surface of magnetite to hematite or to Fe(II) loss after exposure to the physico-chemical conditions of the loop.

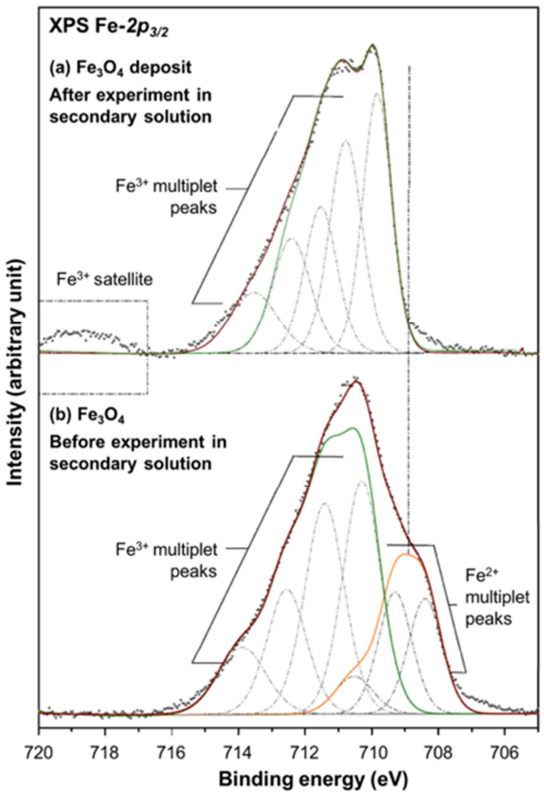

Figure 8: Fe $2p_{3/2}$ spectra of the magnetite oxide deposit after (a) and before (b) exposure to secondary solution without PAA with labelled Fe^{2+} and Fe^{3+} multiplet peaks with Fe $2p_{3/2}$ envelope fitted using Gupta and Sen parameters [31].

XPS analyses have shown that all samples have undergone a degree of oxidation while in the GROZIE loop, as indicated by the Fe^{3+} satellite peaks and the loss of the Fe(II) peaks (Figure 7). The resulting outer layer in the first 10 nm of the sample surface is hypothesized to be hematite for all samples. However as this technique does not surpass the 10 nm of surface depth, the thickness of the outer layer could differ between the samples. It remains to be determined what contribution the presence of PAA has to the formation of hematite oxide layer. TEM analyses were performed on the cross-section of deposit/Inconel 690TT samples to establish if PAA favors the formation of hematite on the magnetite layer at 0.1 $mg.kg^{-1}$ PAA and 10 $mg.kg^{-1}$ PAA. The reference sample without PAA was compared. The results from the imaging done at octahedral peak corners for the tests at 0 $mg.kg^{-1}$ PAA, 0.1 $mg.kg^{-1}$ PAA and 10 $mg.kg^{-1}$ PAA are shown in Figure 9 (a), Figure 9 (b) and Figure 9 (c) respectively.

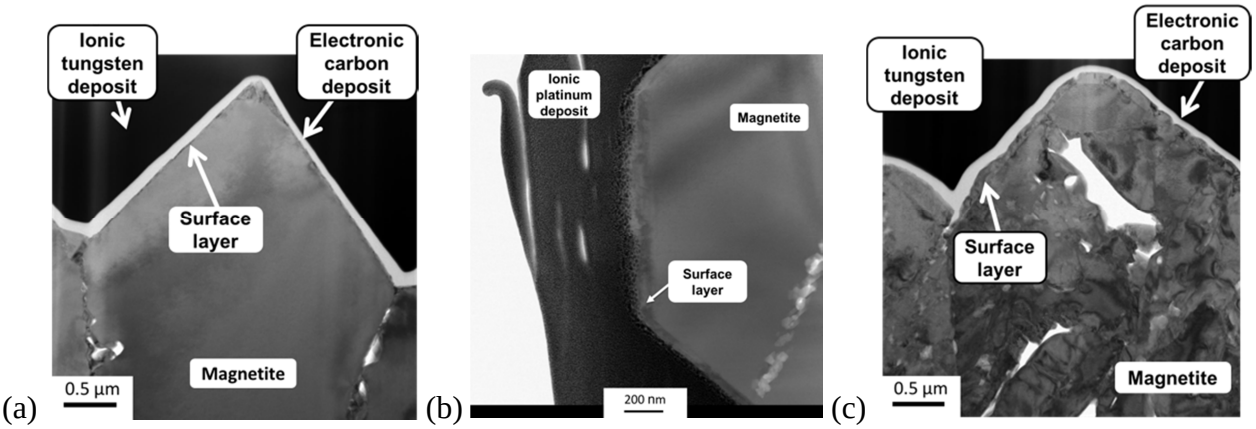

Figure 9: HAADF-STEM images of magnetite octahedra surface with surface layer,

after tests on the Inconel 690TT at 0 $mg.kg^{-1}$ PAA (a), 0.1 $mg.kg^{-1}$ PAA (b) and 10 $mg.kg^{-1}$ PAA (c)

Electronic micro-diffraction patterns were different for the outer surface layer and for the magnetite core layer, meaning a difference in phase or crystallographic orientation. However, the phase observed for the surface layer in the absence and presence of 0.1 $mg.kg^{-1}$ PAA remains to be determined. Two sites were tested by electronic micro-diffraction analyses as shown in Figure 10, one on the surface layer (labeled 1) and the other on the magnetite bulk grain (labeled 2). The indexation of these diffraction patterns gave two different matrix of iron phase. As expected the point labeled 1 was found to be hematite (α-Fe_2O_3), indexed at [110] (Figure 11), while at point 2, the oxide phase was magnetite (Fe_3O_4), indexed in the case of the sample after 0.1 $mg.kg^{-1}$ PAA to be [022] (Figure 12). The indexation of diffraction patterns for all tested sites and different concentrations of PAA are gathered in Table 5 and show the same result for 0 $mg.kg^{-1}$ PAA and 10 $mg.kg^{-1}$ PAA. The simulations created using the software Electron

Diffraction, are presented in Figure 11 (b) and Figure 12 (b) with their corresponding experimental diffraction patterns. The crystallographic parameters used for the identification of the phases were taken from the works by Villars [33].

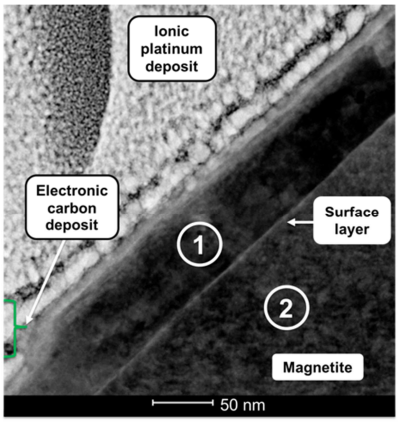

Figure 10: HAADF-STEM image of magnetite octahedra surface with surface layer, showing the selected diffraction locations (after test on the Inconel 690TT at 0.1 mg.kg^{-1} PAA sample)

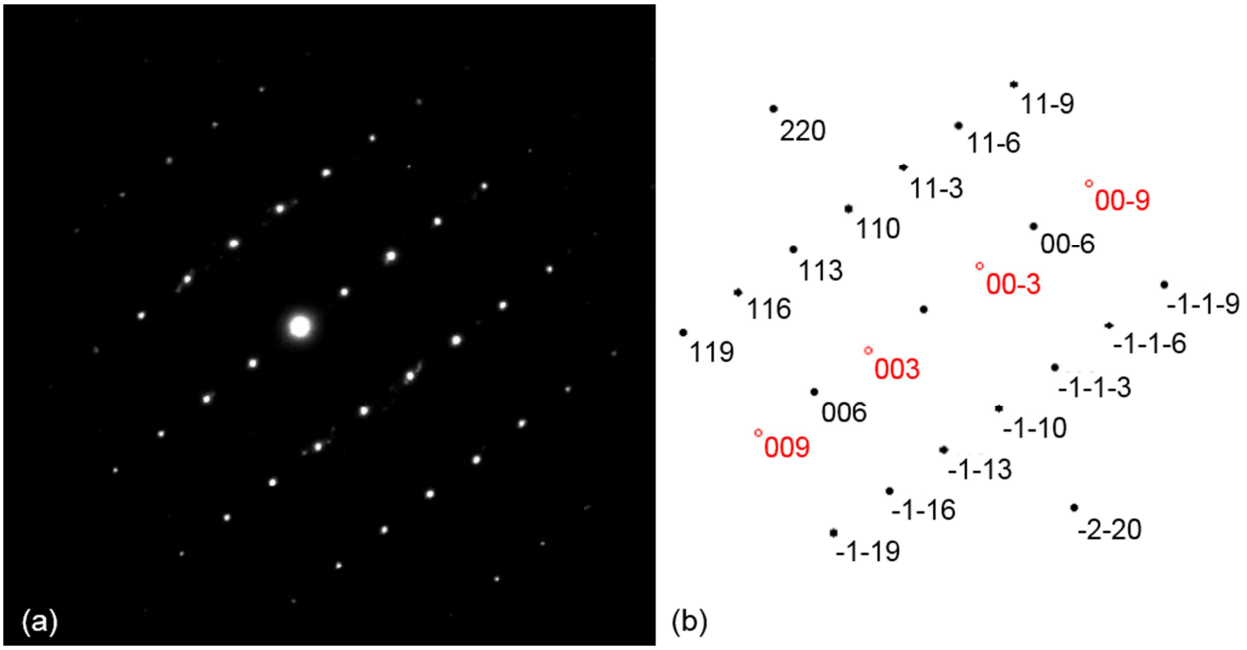

Figure 11: (a) Micro-diffraction of the matrix (position 1 in Figure 10). This diffraction was indexed as [1-10] for hematite. (b) Electron diffraction simulation. The red marks are theoretically off, but are experimentally present due to dynamic effects (possible double diffraction paths).

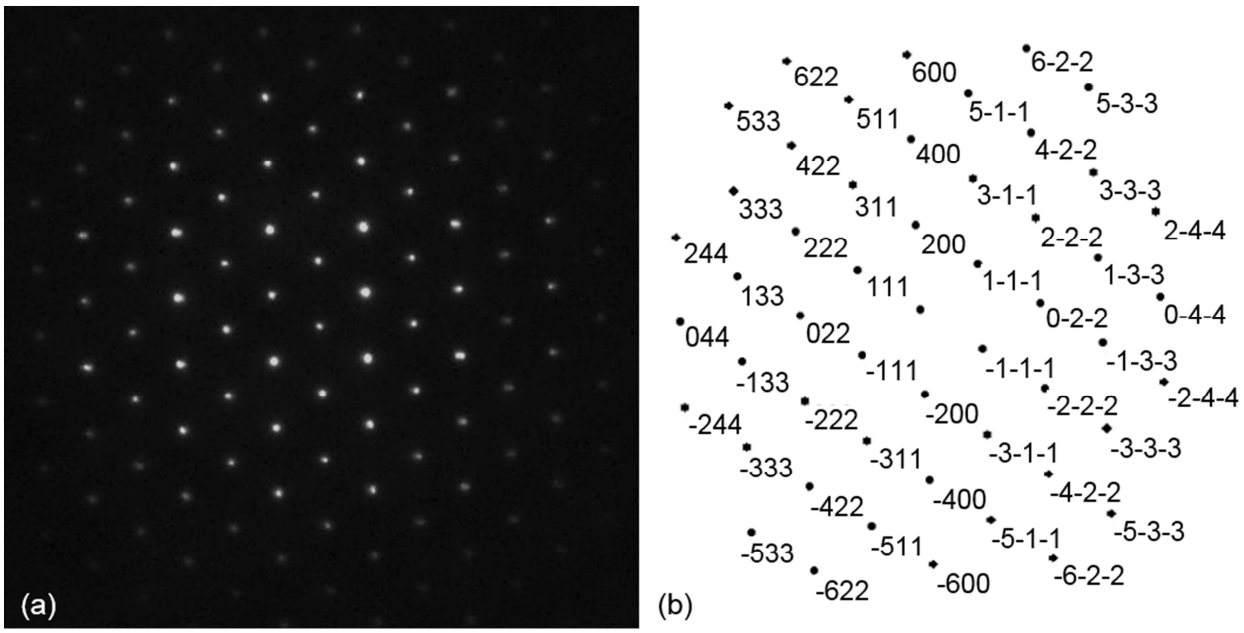

Figure 12: (a) Micro-diffraction of the matrix (position 2 in Figure 10). This diffraction was indexed as [0-22] for magnetite. (b) Electron diffraction simulation.

	Hematite (site 1)	**Magnetite (site 2)**
0	[210]	[101]
0.1	[110]	[022]
10	[110]	[101]

Table 4: Indexation of diffraction patterns for samples tested in the absence and presence of PAA at concentrations 0.1 and 10 mg.kg-1

Thanks to the HAADF-STEM images performed on the samples tested in the absence and in the presence of 0.1 and 10 $mg.kg^{-1}$ PAA, the surface layer thickness was evaluated. An average of measurements was done on two TEM images 20 times for each sample. The results are presented in **Erreur ! Source du renvoi introuvable.**. It was observed that the surface layer thickness formed after exposure to 0.1 $mg.kg^{-1}$ PAA and 10 $mg.kg^{-1}$ PAA was respectively variable between 40 nm and 80 nm and between 58 nm and 171 nm. However, the thickness obtained after the test performed in the absence of PAA ranged between 7 nm to 40 nm. In conclusion, a hematite layer was formed on all samples. An increase in the hematite layer thickness was measured with an increase of PAA

concentration. Moreover, the hematite layers were thicker and more distorted on the octahedra peak corners relative to the octahedra base. From comparison of the samples after the three PAA concentrations tested, it is suggested that the hematite layer formed on the samples (Figure 4 and Figure 5) increases in thickness with increasing concentration of PAA.

	Measured thickness (nm)		
PAA concentration ($mg.kg^{-1}$)	**Minimum**	**Maximum**	**Average***
0	7	40	18
0.1	40	80	59
10	58	171	109

*Average based on 40 measurements from 2 images

Table 5: Average of measured thicknesses of the thin oxide layer formed on magnetite after tests in the absence and in the presence of 0.1 and 10 $mg.kg^{-1}$ PAA

The TEM results demonstrate that the interaction of PAA with the magnetite layer results in the attack of the octahedral peaks and in the increase of formation of hematite on the surface of the oxide layer. It can be suggested that there is an epitaxial growth of hematite onto the magnetite crystallites from the determined indexes, for hematite [1-10] and magnetite [0-22]. The aforementioned effect occurs from the minimum tested concentration, 0.1 $mg.kg^{-1}$ PAA and the layer increase in thickness with increasing PAA concentration. This was seen in the TEM observations (Figure 9) but also with XRD analyses of samples exposed to 10 $mg.kg^{-1}$ PAA (Figure 6).

Until now, the results have shown the curative effect of PAA on pre-existing magnetite layer, with a preferential attack of the octahedral peak corners and an increase in the formation of a hematite layer on the surface. The next step is to determine if PAA remains on the oxide surface after interaction.

XPS analyses were performed on the electrochemical deposits after the exposure tests to 0, 0.1 and 10 $mg.kg^{-1}$ PAA. Narrow scans were performed to analyze carbon and oxygen, two atoms present in the PAA molecule. As a reference, a synthetic PAA sample was prepared by spin-coating 120×10^{-6} l PAA solution (molecular weight: 100,000 $g.mol^{-1}$, 35 weight % in water) onto a glass substrate (spin acceleration: 2000 $rpm.s^{-1}$, spin speed: 6000 rpm and duration: 15 s), to determine the shape and intensity of the PAA carbon spectrum. The spectrum was fitted by the

three peaks observed by Louette *et al.* [34]: two C-C bond peaks (labeled 1 and 2 in Figure 13) and the carboxyl group (-COOH) bond (labeled 3 in Figure 13). The carboxyl group was of great interest in these scans as carboxylate is responsible for the complexation of PAA with iron oxides, as was shown in references [22–26].

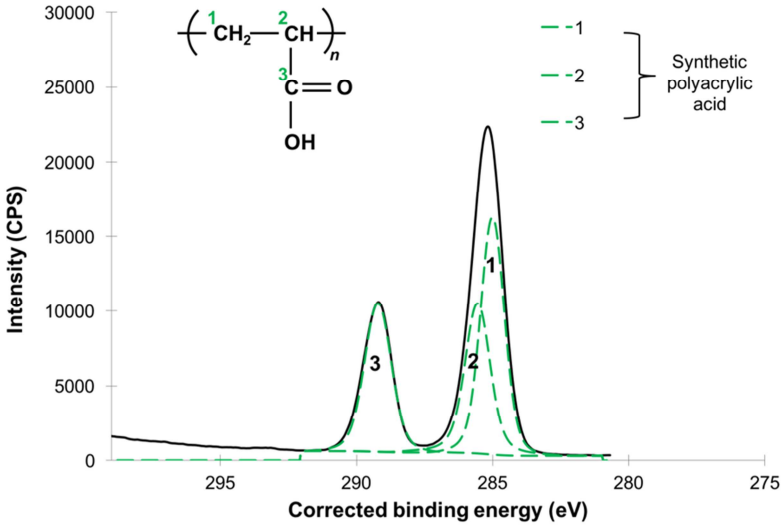

Figure 13: Carbon 1s spectrum of PAA (MW = 100,000 g.mol^{-1})

Analyses of the C 1s peaks for all tested samples (Figure 14) showed the presence of a high intensity C-C bond peak (labeled 1 in Figure 13) as well as a weak signal of the COOH peak (labeled 3 in Figure 13). These peaks were hypothesized to be caused by either the presence of PAA (peaks 1 and 3, Figure 13) on the surface of the sample and/or by carbon pollution. However comparing all peaks to a reference electrochemically deposited sample, not placed in the GROZIE loop shows clearly that this peak is likely due to a carbon pollution. This is further indicated by XPS analyses on the synthetic PAA shown in Figure 13.

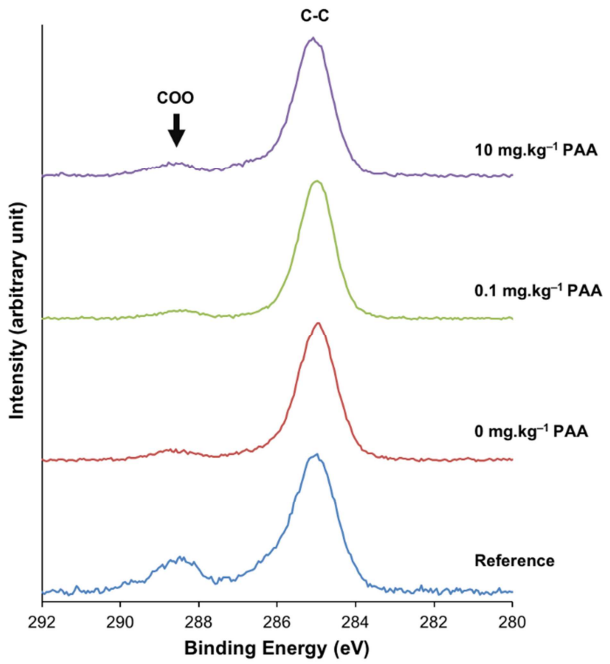

Figure 14: Carbon 1s spectra for the reference sample and samples tested in the presence of 0 mg.kg^{-1} PAA, 0.1 mg.kg^{-1} PAA and 10 mg.kg^{-1} PAA for Inconel 690TT samples.

To quantify if there was an increase in the carboxylic carbon peaks (Figure 14) after exposure to PAA, the ratio of the quantified atomic percent of C 1s peak belonging to carboxylic carbon (-COOH) to a Fe $2p_{3/2}$ peak (corresponding to oxidized iron) was calculated. As shown previously, the Fe $2p_{3/2}$ peak did not change with each test and thus would not influence the ratio. The background of the Fe $2p_{3/2}$ envelop was subtracted using the Shirley approximation. The carbon (-COOH) peak was fitted using the reference data from Louette *et al.* [34]. **Erreur ! Source du renvoi introuvable.** shows the average intensities of each test and the calculated ratios for Inconel 690TT. In both cases, the –COOH peak intensity after testing with and without PAA was smaller than that obtained for the reference, not placed in the loop. Thus, the –COOH peak intensity cannot be attributed to the presence of PAA on the extreme surface and could be due to carbon pollution on the reference sample. However, the ratio of the Fe $2p_{3/2}$ intensity to the COOH intensity decreased significantly with increasing values of PAA concentration.

	Reference		**0 mg.kg^{-1} PAA**		**0.1 mg.kg^{-1} PAA**		**10 mg.kg^{-1} PAA**	
	Fe $2p_{3/2}$ (Fe 2p)	COOH (C 1s)	Fe $2p_{3/2}$ (Fe 2p)	COOH (C 1s)	Fe $2p_{3/2}$ (Fe 2p)	COOH (C 1s)	Fe $2p_{3/2}$ (Fe 2p)	COOH (C 1s)
Average	79.3	20.8	94.1	5.9	93.7	6.3	90.1	9.9

Standard Deviation	-	-	3.7	3.7	0.9	0.9	5.0	5.0
Ratio of Average	3.8		15.9		14.9		9.1	

Table 6: Evolution of Fe $2p_{3/2}$: COOH intensity ratio with PAA concentration for Inconel 690TT (in atomic %)

The results suggest that no significant PAA molecules remained on the surface after interaction with the magnetite deposit, considering the ratio of the Fe $2p_{3/2}$ to the C1s – carboxylic acid peak. It can be hypothesized that the PAA does not remain on the magnetite surface after testing because it has been thermally degraded. At the GROZIE testing temperature, 275 ºC, it was determined previously [29], that PAA is 50 % thermally degraded after 20 min of residence time. This is further indicated by the results by Johansson *et al.* [35] who studied the interaction (adsorption) of carboxylic acid on oxidized metals by XPS at room temperature. Several differences exist between the current study and that by Johansson *et al.* [35], such as the residence time, temperature and solution pH, however they observed a clear increase in the C 1s peak and a decrease in the Fe 2p and O 1s peaks after the adsorption in 0.5×10^{-3} M solution of carboxylic acid containing molecules for 3 hours on hematite (α-Fe_2O_3) oxide layer.

4. Conclusion

In conclusion, we have shown the partial curative effect of PAA on pre-formed magnetite layers in physico-chemical conditions close to those encountered in SGs of PWRs. It has been shown by *in-situ* iron concentration measurements that PAA has a curative effect on the magnetite layer. This conclusion was most apparent for the test at the highest PAA concentration (10 $mg.kg^{-1}$ PAA). A linear evolution of the iron concentration with the PAA content between 0.1 $mg.kg^{-1}$ and 10 $mg.kg^{-1}$ was found. Moreover, the interaction mechanism of PAA with magnetite has been determined. Initial results by SEM showed a localized diminution of the magnetite octahedral crystallite peak corners and an attack of the lateral facets for samples tested with PAA in the GROZIE loop. This was only apparent when the samples were exposed to PAA. Further SEM analyses of samples from tests at 1 and 10 $mg.kg^{-1}$ PAA provided evidence for the formation of an outer layer, localized mostly on the octahedral peak corners.

Analyses of the surface oxide layer using XRD indicated the possibility of a change in the oxide phase from magnetite to hematite after exposure to the highest concentration of PAA (10 $mg.kg^{-1}$ PAA). XRD analyses at 0.1 and 1 $mg.kg^{-1}$ PAA did not show this phase change, but this was due to the detection limit of this method. XPS analyses of the samples have indicated that all samples underwent an oxidation after exposure to the circuit chemistry, however the contribution of PAA was not conclusive. The phase of the surface layer present on the

magnetite octahedra was undoubtedly determined by TEM and electron micro-diffraction analyses of samples tested at 0, 0.1 and 10 $mg.kg^{-1}$ PAA. The surface layer was determined to have an epitaxial relationship with the underlying magnetite surface. It was observed to be thicker at the octahedral peak corners. These analyses confirmed the presence of hematite on all tested samples. Moreover, the hematite layer appeared to increase in thickness with increasing concentrations of PAA. Two possible mechanisms for hematite layer formation have been considered, namely direct oxidation of magnetite or iron (II) complexation by PAA [36]. Finally, XPS analyses suggested that the PAA molecules do not remain on the extreme surface of the oxide layer after experimentation. It was hypothesized that it is due to its thermal degradation at the tested temperature.

Acknowledgements

This work was funded by EDF (Electricity of France) and CEA (Atomic Energy Commission). The authors acknowledge the Radiolysis and Organic Matter Laboratory (LRMO) at CEA Saclay, where an experimental device was specifically adapted for this study.

5. References

[1] C. Goujon, T. Pauporté, A. Bescond, C. Mansour, S. Delaunay, and J.-L. Bretelle, “Effects of curative and preventive chemical cleaning processes on fouled steam generator tubes in nuclear power plants,” *Nuclear Engineering and Design*, vol. 323, no. Supplement C, pp. 120–132, 2017.

[2] H. Kawamura, K. Fujiwara, H. Kanbe, H. Hirano, H. Takiguchi, K. Yoshino, S. Yamamoto, T. Shibata, and K. Ishigure, “Applicability of Chemical Cleaning Process to Steam Generator Secondary Side, (III),” *Journal of Nuclear Science and Technology*, vol. 43, no. 6, pp. 655–668, 2006.

[3] C. Gasnier and D. H. Lister, “The effects of chemical additives on magnetite deposition in boiling heat transfer,” 2013.

[4] C. Laire, D. Ceursters, B. S., R. Delporte, S. Coart, and R. Lecocq, “First Steam Generator Cleanup Application with Dispersant at Doel 3,” in *Nuclear Plant Chemistry Conference, Sapporo, Japan*, 2014, no. 10077.

[5] S. Mercier, G. Corredera, M. Alves-Vieira, C. Mansour, and D. You, “EDF plan for a dispersant injection trial,” in *Nuclear Plant Chemistry Conference*, 2012, no. P2–07, p. 11.

[6] P. Robbins, “Dispersants for Tube Fouling Control - Volume 2: Short-Term Trial at ANO-2,” EPRI, 1003144, 2001.

[7] P. Robbins, “Dispersants for Tube Fouling Control - Volume 1: Qualification for a Short-Term Trial at ANO-2,” EPRI, 1003144, 2001.

[8] R. W. Staehle and J. A. Gorman, “Progress in understanding and mitigating corrosion on the secondary side in PWR steam generators,” ASM Specialty Handbook, 1994.

[9] C. Goujon, T. Pauporté, C. Mansour, S. Delaunay, and J.-L. Bretelle, “Electrochemical Deposition of Thick Iron Oxide Films on Nickel Based Superalloy Substrates,” *Electrochimica Acta*, vol. 176, pp. 230–239, 2015.

[10] D. Carlier, C. Terrier, C. Arm, and J. . Ansermet, “Preparation and magnetic properties of Fe3O4 nanostructures grown by electrodeposition,” *Electrochem. Solid-State Lett.*, vol. 8, p. C43, 2005.

[11] F. Carré and C. Renault, *Réacteurs nucléaires du futur*. Techniques de l’ingénieur, 2005.

[12] S. Chatman, A. J. G. Noel, and K. M. Poduska, “Tuning magnetic hysteresis of electrodeposited Fe3O4,” *J. Appl. Phys.*, vol. 98, p. 113902, 2005.
[13] H. M. Kothari, E. A. Kulp, S. J. Limmer, P. Poizot, E. W. Bohannan, and J. A. Switzer, “Electrochemical deposition and characterization of Fe3O4 films produced by the reduction of Fe(III)-triethanolamine,” *J. Mater. Res.*, vol. 21, pp. 293–301, 2006.
[14] L. Martinez, D. Leinen, F. Martin, M. Gabas, and J. R. Ramos-Barrado, “Electrochemical growth of diverse iron oxide (Fe3O4, alpha-FeOOH, and gamma-FeOOH) thin films by electrodeposition potential tuning,” *J. Electrochem. Soc.*, vol. 146, pp. D126–D133, 2007.
[15] S. Peulon, H. Antony, L. Legrand, and A. Chaussé, “Thin layers of iron corrosion products electrochemically deposited on inert substrates: synthesis and behavior,” *Electrochemica Acta*, vol. 49, no. 17–18, pp. 2891–2899, 2004.
[16] T. A. Sorenson, S. A. Morton, D. G. Waddill, and J. A. Switzer, “Epitaxial electrodeposition of Fe3O4 thin films on the low-index planes of gold,” *J. Am. Chem. Soc*, vol. 124, pp. 7604–7609, 2002.
[17] C. Terrier, M. Abid, C. Arm, S. Serrano-Guisan, L. Gravier, and J. P. Ansermet, “Fe3O4 nanowires synthesized by electroprecipitation in templates,” *J. Appl. Phys.*, vol. 98, p. 086102, 2005.
[18] T. Pauporté, F. Andolfatto, and R. Durand, “Some electrocatalytic properties of anodic iridium oxide nanoparticles in acidic solution,” *Electrochimica Acta*, vol. 45, no. 3, pp. 431–439, 1999.
[19] T. Pauporté, D. Aberdam, J. L. Hazemann, R. Faure, and R. Durand, “X-ray Absorption in Relation to Valency of Iridium in Sputtered Iridium Oxide Films,” *J. Electroanal. Chem.*, vol. 465, pp. 88–95, 1999.
[20] M. Roy, V. Mertens, and D. You, “Caractérisation du produit Optisperse PWR-6610 et effet de l’Acide PolyAcrylique (APA) contenu dans ce produit sur le fer.,” CEA Saclay, DPC/SECR/NT/2013/044 Indice A, 2013.
[21] M. Roy, A. Gangloff, V. Mertens, and D. You, “Effet curatif de l’Acide PolyAcrylique (APA) contenu dans l’Optisperse PWR-6610 sur des dépôts d’oxyde de fer,” CEA Saclay, DPC/SECR/NT/2015/040 Indice A, 2015.
[22] S. Crisp, H. J. Prosser, and A. D. Wilson, “An infra-red spectroscopic study of cement formation between metal oxides and aqueous solutions of poly (acrylic acid),” *J. Mater. Sci.*, vol. 11, no. 1, pp. 36–48, 1976.
[23] R. Baigorri, J. M. Garcia-Mina, and G. Gonzalez-Gaitano, “Supramolecular association induced by Fe(III) in low molecular weight sodium polyacrylate,” *Colloids Surf A Physicochem Eng Asp*, vol. 292, no. 2–3, pp. 212–216, 2007.
[24] F. Jones, J. B. Farrow, and W. V. Bronswijk, “An infrared study of a polyacrylate flocculant adsorbed on hematite,” *Langmuir*, vol. 14, no. 22, pp. 6512–6517, 1998.
[25] L. J. Kirwan, P. D. Fawell, and W. V. Bronswijk, “In situ FTIR-ATR examination of poly(acrylic acid) adsorbed onto hematite at low pH,” *Langmuir*, vol. 19, no. 14, pp. 5802–5807, 2003.
[26] T. Sugama, L. E. Kukacka, and N. Carciello, “Nature of interfacial interaction mechanisms between polyacrylic acid macromolecules and oxide metal surfaces,” *Journal of Materials Science*, vol. 19, pp. 4045–4046, 1984.
[27] A. C. Joshi, A. L. Rufus, S. Suresh, P. Chandramohan, S. Rangarajan, and S. Velmurugan, “Characterization of the oxide formed in the presence of poly acrylic acid over the steam generator structural materials of nuclear power plants,” *Journal of Nuclear Materials*, vol. 437, pp. 139–148, 2013.
[28] P. Artola, B. Rousseau, C. Clavaguera, M. Roy, D. You, and G. Plancque, “Preventing iron (II) precipitation in aqueous systems using Polyacrylic acid: some molecular insights,” *Phys. Chem. Chem. Phys.*, 2018.
[29] C. Lamouroux, D. You, G. Plancque, M. Roy, C. Laire, and P. Schnongs, “Assessment of the PolyAcrylic Acid for an Ammonia Water Treatment and for Alloy 800NG SG Tube Material in Pressurized Water Reactors,” in *Nuclear Plant Chemistry Conference*, 2012, p. 9.
[30] R. P. Gupta and S. K. Sen, “Calculation of multiplet structure of core p-vacancy levels,” *Phys. Rev. B*, vol. 10, no. 1, pp. 71–77, Jul. 1974.
[31] R. P. Gupta and S. K. Sen, “Calculation of multiplet structure of core p -vacancy levels. II,” *Phys. Rev. B*, vol. 12, no. 1, pp. 15–19, Jul. 1975.
[32] A. P. Grosvenor, B. A. Kobe, M. C. Biesinger, and N. S. McIntyre, “Investigation of multiplet splitting of Fe 2p XPS spectra and bonding in iron compounds,” *Surface and Interface Analysis*, vol. 36, pp. 1564–1574, 2004.
[33] P. Villars, *Pearson’s handbook: crystallographic data for intermetallic phases*. ASM international, 1997.
[34] P. Louette, F. Bodino, and J. J. Pireaux, “Poly(acrylic acid) (PAA) XPS Reference Core Level and Energy Loss Spectra,” *Surf. Sci. Spectra*, vol. 12, pp. 22–26, 2005.

[35] E. Johansson and L. Nyborg, “XPS study of carboxylic acid layers on oxidized metals with reference to particulate materials,” *Surf. Interface Anal.*, vol. 35, no. 4, pp. 375–381, 2003.
[36] R. D’Angelo, “The effects of dispersants on the fouling and the blockage deposits in pressurized water reactor steam generators,” Université Pierre et Marie Curie, 2016.